

# Affine and Euclidean Geometric Heat Equation for Anisotropic Smoothing

Maxime Descoteaux<sup>†</sup>

<sup>†</sup>School of Computer Science  
McGill University  
ID no: 9932537  
email: mdesco@cim.mcgill.ca

April 28, 2003

## Abstract

The study of geometric flows on 2D and 3D objects has received much attention in the past decade. The main applications of some of these evolution equations are for smoothing and for multi-scale representations. In this work, we study the geometric smoothing of curves and surfaces via the geometric heat equation known as the deformation by local curvature. We emphasize the paper on the affine analogue of this flow and its formulation in terms of Euclidean curvature and normal. We investigate the key mathematical properties of both the Euclidean and the affine geometric heat equation that make them sensible smoothing methods. We know that the Euclidean geometric heat equation corresponds to the *shortening flow* and we discuss the analogue in affine geometry. We question a statement made in the publications by Sapiro, Tannenbaum and others and try to suggest a more valid one. Our main concern is the application of the geometric flows on angiograms and MRI medical images. We present the implementation of the two different flows and nice results of both evolution method. We clearly see the advantages of the implemented flows. Both approaches have the property of smoothing along structure of images and not across them. In our medical imaging setting, this is excellent as we preserve blood vessels while removing artifacts and speckle noise.

# 1 Introduction

Medical images very often contain noise and artifacts which complicate the image analysis. It interferes badly with the derivative and gradient computation which make edge detection, segmentation or other image processing application based on local properties of the image imprecise and less effective. Typically, to resolve this issue, we need to preprocess the image with a few iterations of some smoothing method. But which smoothing approach is the best to use? The answer to this question obviously depends on the application. In our case, we want to preserve important structure of the image like blood vessels while removing artifacts and reducing noise. The first and most popular smoothing method candidate is using a Gaussian kernel operator. It is well-known that this smoothing corresponds to the heat equation which has the property of smoothing equally in all directions [1]. Hence, this isotropic procedure smooths across blood vessels and is unusable and bad in our application. It is still interesting to point out that Koenderink showed it is the only sensible way to smooth images with a linear operator, by demanding that structure is not created (no new extremas) in the evolution and that operations are homogeneous in space and direction [1,[48,50]]. In the vision literature these properties are termed as *causality*, *homogeneity* or *semi-group* and *isotropy*.

We are interested in finding a smoothing approach that preserves the first two properties but that does not necessarily smooths equally in all direction nor forced to be a linear operator. This paper will explore two such methods based on to the geometric heat equation. As we will see later, the two methods have very similar properties. One approach is the well-known *shortening flow* in Euclidean geometry and the other is a similar flow but derived in affine geometry by Sapiro and Tannenbaum in [6], [7]. In [1], Siddiqi *et al.* show that the geometric heat equation has the wanted causality and semi-group properties but not the isotropy characteristic. It is instead very similar to anisotropic diffusion. In fact, it can be shown that the diffusion term of the evolution equation is zero in the direction of brightness gradient. Thus, the smoothing is along boundaries and not across them. The edges are left intact. As we will mathematically investigate later, the geometric heat equation has many desirable smoothing properties that make it a more interesting and a better candidate for our application than Gaussian smoothing.

This paper will explore variations of the geometric heat equation. It is organized as follows. Section 2 reviews the geometric heat equation in Euclidean geometry and establishes the analogue affine equation. The flows are presented in both 2D and 3D space. We also contest a statement made by Sapiro and Tannenbaum and suggest a correction to the statement. Then, Section 3 explores the interesting mathematics publications that state and prove the various desirable properties of the two parabolic partial differential evolution equations. In Section 4, we discuss the validity and stability of the level set methods for smoothing images. In Section 5, the implementation details and issues are presented. Finally, in Section 6, we illustrate the flows on numerous shapes and volumes before showing results on medical images. We try to note the differences and attempt a comparison between the Euclidean and affine smoothing flow in Section 7.

## 2 The Geometric Heat Equation

In this section, we show how the geometric heat equation arises from specific evolution equations. First, from a curvature deformation in 2D and a similar deformation on 3D surfaces in Euclidean geometry. Then, we explore the corresponding affine geometric flows. To do so, we introduce the basic differential geometry tools needed. There are important differences between the two geometries but the flows turn out to be quite similar and all have the desired property of smoothing along edges and not across them. In this sense, they are all cases of the geometric heat equation. The next section will investigate in more depth the key mathematical properties of the flows.

### 2.1 Euclidean Shortening Flow

In Euclidean space, the equations that give rise to the geometric heat equations are the curvature deformation flow for a 2D curve,  $\mathcal{C}$ , and its 3D extension, the mean curvature deformation flow for a surface,  $\mathcal{S}$ ,

$$\frac{\partial \mathcal{C}}{\partial t} = \kappa \vec{N} \quad , \quad \frac{\partial \mathcal{S}}{\partial t} = \kappa \vec{N}$$

In the 3D case,  $\kappa$  is the mean curvature of the surface defined in terms of principal curvatures  $\kappa_1$  and  $\kappa_2$  [13],

$$\kappa = \frac{\kappa_1 + \kappa_2}{2}$$

It is well-known in the literature that the 2D evolution is the Euclidean curve shortening flow in the sense that perimeter shrinks as fast as possible. In fact, it is possible to obtain this flow from first principle by minimizing the proper length functional [15]. But what is the link with the heat equation? The heat equation is

$$\psi_t = \psi_{rr} + \psi_{r'r'}$$

for any  $r$  and  $r'$  perpendicular. In our case, the  $r'$  term is in direction of the gradient to the curve and it vanishes if the signed distance function [1] is used as higher dimensional embedding function. Also, using level set formulation [1],[5], the curve flow can be rewritten as

$$\psi_t = \psi_{rr}$$

where  $r$  is perpendicular to  $\nabla\psi$ , i.e.,  $r$  is along the curve. This is derived in [1]. Hence, the flow does not smooth in all direction. It does not smooth across structure but along. Therefore, the curvature deformation flow is anisotropic and a geometric case of the heat equation.

### 2.2 Affine 2D Analogue

We now seek a flow in affine geometry with similar properties as the Euclidean shortening flow. We want to derive an affine curvature deformation flow analogue to the previous

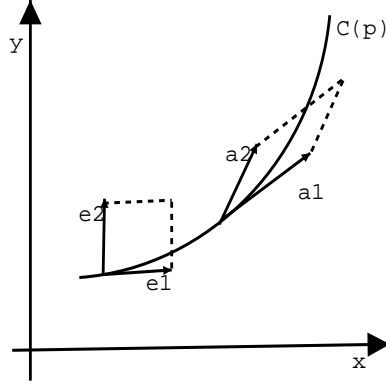


Figure 1: Basic Affine Differential Geometry

section. We first give the basic concepts of affine differential geometry in the plane and then extend it to 3D affine space.

A general affine transformation is given by  $Y = XA + B$ , where  $A$  is a  $2 \times 2$  invertible matrix with positive determinant and  $B$  is a translation vector in  $R^2$ . Transformations of that type form a group called *group of proper affine motions* [13]. In our application, we restrict the determinant of  $A$  to be equal to one to obtain an invariant transformation. Thus, from our usual orthogonal Frenet frame  $\{e_1, e_2\}$  in Euclidean differential geometry, we want a frame  $\{a_1, a_2\}$  defined at each point of the curve  $C(p)$ , where  $a_1$  is always tangent to the curve. A natural choice of frame is  $\{C_p, C_{pp}\}$ , as  $C_p$  is always tangent to  $C(p)$ . However, note that for an arbitrary parametrization (not arc-length),  $C_{pp}$  is not necessarily orthogonal to  $C_p$ . Hence,  $\{a_1, a_2\} = \{C_p, C_{pp}\}$  defines an oblique frame, as seen in Figure 1. Now, we look for a parametrization  $s$ , the *affine arc-length*, of the curve such that the area of the parallelogram defined by this oblique frame is one. We will then have an area-preserving affine transformation of the Frenet frame.

Let  $[C, C']$  denote the  $2 \times 2$  determinant where the first column is defined by components of  $C$  and the second column by those of  $C'$ , i.e.,

$$[C, C'] = \begin{vmatrix} x & x' \\ y & y' \end{vmatrix}$$

Hence, we define a parameter  $s$  such that the area of the parallelogram is one,  $[C_s, C_{ss}] = 1$ . Using the chain rule, we obtain the following derivation,

$$\begin{aligned} [C_p, C_{pp}] &= x_p y_{pp} - x_{pp} y_p \\ &= \frac{dx}{ds} \frac{ds}{dp} * \frac{d^2 y}{ds^2} \left(\frac{ds}{dp}\right)^2 - \frac{dy}{ds} \frac{ds}{dp} * \frac{d^2 x}{ds^2} \left(\frac{ds}{dp}\right)^2 \\ &= \left(\frac{ds}{dp}\right)^3 [C_s, C_{ss}] \\ &= \left(\frac{ds}{dp}\right)^3 \end{aligned} \tag{1}$$

From this derivation, we get the *affine metric*

$$g = [C_p, C_{pp}]^{\frac{1}{3}} \tag{2}$$

and the *affine arc-length* parameter

$$s(p) = \int_0^p g(\xi) d\xi \quad (3)$$

We also define the *affine tangent* to be  $C_s$ , the *affine normal*  $C_{ss}$  and the *affine curvature* to be  $\mu = [C_{ss}, C_{sss}]$  [13]. From equation (2), (3) and the chain rule we easily get the following relevant relations

$$ds = g dp \quad (4)$$

$$C_s = C_p \frac{dp}{ds} \quad (5)$$

$$\begin{aligned} C_{ss} &= C_{pp} \left(\frac{dp}{ds}\right)^2 + C_p \frac{d^2p}{ds^2} \\ &= C_{pp} \frac{1}{g^2} - C_p \frac{g_p}{g^3} \end{aligned} \quad (6)$$

Now, we investigate the affine analogue of the curve shortening flow. In Euclidean differential geometry, the flow is  $\mathcal{C}_t = \kappa \vec{N} = C_{ss}$ , where  $s$  is the arc-length parameter [13]. In affine geometry, this motivates the choice of evolution  $\mathcal{C}_t = C_{ss}$ , where  $s$  is now the affine arc-length. However, we must deal with the fact that basic affine differential geometry is only defined for convex curve as the affine metric  $g$  cannot equal zero. If so, the affine normal is undefined and all definitions collapse. For non-convex curves,  $g$  only vanishes at inflection points of a curve. Thus, we modify the flow as proposed in [8] and [9]

$$\mathcal{C}_t = \begin{cases} 0 & \text{at inflection points} \\ C_{ss} & \text{otherwise} \end{cases} \quad (7)$$

Now, we want to express the affine normal vector,  $C_{ss}$ , in terms of Euclidean quantities. We use equation (6) to do so. We choose the parameter  $p$  to be the Euclidean arc-length. Thus,  $C_p = \vec{T}$  and  $C_{pp} = \kappa \vec{N}$ , where  $\vec{T}$  and  $\vec{N}$  are the Euclidean unit tangent and normal respectively. Hence,

$$\begin{aligned} g &= [C_p, C_{pp}]^{\frac{1}{3}} \\ &= [\vec{T}, \kappa \vec{N}]^{\frac{1}{3}} \\ &= \kappa^{\frac{1}{3}} [\vec{T}, \vec{N}]^{\frac{1}{3}} \\ &= \kappa^{\frac{1}{3}} \quad \text{since } \vec{T} \text{ and } \vec{N} \text{ are orthogonal unit length vectors} \end{aligned}$$

Therefore, we have

$$\begin{aligned} C_{ss} &= C_{pp} \frac{1}{g^2} - C_p \frac{g_p}{g^3} \\ &= \kappa^{\frac{1}{3}} \vec{N} - \frac{\kappa_p}{3\kappa^{\frac{2}{3}}} \vec{T} \end{aligned} \quad (8)$$

It is well-known in curve evolution theory that the tangential component of the velocity vector affects only the parametrization of the family of curves in the evolution, not their shape [7]. This fact combined with the fact that curvature,  $\kappa$ , vanishes at inflection points, implies that the affine flow given by (7) is geometrically equivalent to

$$\mathcal{C}_t = \kappa^{\frac{1}{3}} \vec{N} \quad (9)$$

This flow is what all the the literature on affine evolutions claim to be the affine analogue of the curve shortening flow in Euclidean space. What is the analogy? Siddiqi *et. al.* [15] have showed that curvature deformation in the normal direction is the fastest way to shrink the length functional of a curve in Euclidean geometry. Now, in affine geometry, the claimed analogue is the functional is affine length and the fastest way to shrink it is the evolution in the affine normal direction which corresponds to an Euclidean curvature deformation in the Euclidean normal direction.

We have strong issues with this claim and the way it is proved in [7]. First, we consider the derivation on p.105 of [7]. We carefully verified that every step of the proof is valid. It is indeed correct until the last statement

$$\begin{aligned} L'(t) &= \oint gdp \\ &\vdots \\ &= -\frac{2}{3} \int_0^{L(t)} \mu[C_s, C_t] ds \end{aligned} \tag{10}$$

Now, Sapiro and Tannenbaum state “if  $\mathcal{C}_t = C_{ss}$ , we obtain  $[C_s, \mathcal{C}_t] = 1$ , which gives the direction of the most rapid decrease for the affine perimeter”. The first part is true but the last part is false. From derivation (10), the gradient flow which will decrease the affine length as quickly as possible is the one that will maximize the area of the parallelogram defined by  $[C_s, C_t]$ . Setting  $\mathcal{C}_t$  in the direction of the affine normal is not maximizing that area. What is the maximum area enclosed by two vectors,  $\vec{v}$  and  $\vec{u}$ ? It is maximum when the sine of the angle between the two vectors is one as

$$[\vec{v}, \vec{u}] = |u||v|\sin\theta_{uv}$$

Hence,  $\vec{v}$  and  $\vec{u}$  have to be orthogonal. However, we know that  $C_{ss}$  and  $C_s$  are not perpendicular. Therefore, something is wrong when they say that setting  $\mathcal{C}_t = C_{ss}$  gives the direction of most rapid decrease of the affine perimeter.

Lets compute the expression in the integral of equation (10). We need the straight forward fact that

$$[C_s, C_{ss}] = 1 \implies [C_s, C_{sss}] = 0 \implies x_s y_{sss} = y_s x_{sss} \tag{11}$$

So,

$$\begin{aligned} \mu[\mathcal{C}_t, C_s] &= [C_{ss}, C_{sss}][\mathcal{C}_t, C_s] \\ &= (x_{ss}y_{sss} - x_{sss}y_{ss})(x_t y_s - x_s y_t) \\ &= x_t y_s x_{ss} y_{sss} - y_t x_s x_{ss} y_{sss} + x_s y_t y_{ss} x_{sss} - x_t y_s y_{ss} x_{sss} \\ &= x_t y_{sss} [C_s, C_{ss}] - y_t x_{sss} [C_s, C_{ss}] \quad \text{from (11)} \\ &= [\mathcal{C}_t, C_{sss}] \\ &= \mu \quad \text{if } \mathcal{C}_t = C_{ss} \end{aligned} \tag{12}$$

Hence, we believe that the statement should be corrected and stated as “setting the curve evolution corresponding to the gradient flow  $\mathcal{C}_t = C_{ss}$  decreases the affine length according to its affine curvature. In this sense, the affine version is analogue to the Euclidean flow shrinking a curve by its Euclidean curvature. It is not correct to claim, as in most papers [8-14], that the analogy between Euclidean and the affine geometric heat equation is based on the *shortening flow*. We have argued that the affine curve evolution is not necessarily the fastest way to shrink the affine perimeter.

	Euclidean Geometry	Affine Geometry
2D	$\mathcal{C}_t = \kappa \vec{N}$	$\mathcal{C}_t = \kappa^{\frac{1}{3}} \vec{N}$
3D	$\mathcal{S}_t = \kappa_{\text{mean}} \vec{N}$	$\mathcal{S}_t =  \kappa_{\text{gaussian}} ^{\frac{1}{4}} \vec{N}$

Table 1: Geometric Heat Evolution Equations in Euclidean and Affine Geometry

### 2.3 3D Affine Evolution

In this section, we state the 3D extension to the affine curve evolution  $\mathcal{C}_t = \kappa^{\frac{1}{3}} \vec{N}$  discussed previously. We want to find an affine deformation flow based on the principal curvatures of the surface. The 3D affine differential geometry and setting up the problem is more complicated than the 2D case. Section 4 and 5 of [10] go through the main steps of the derivation. It turns out that the simplest possible affine surface evolution is moving every point of the surface according to the Gaussian curvature raised to some exponent. The Gaussian curvature of a surface is the product of the two principal curvature,  $\kappa = \kappa_1 \kappa_2$ . Why the Gaussian curvature? Analogous to the inflection points issue in 2D, it resolves the “non-existence” problem of 3D affine differential geometry at parabolic points, where one of the two principal curvature vanishes. Thus, using the Gaussian curvature in the flow as opposed to mean curvature assures that parabolic points stay fixed. Also, as we will see in Section 4, the Gaussian curvature has a very convenient and simplified level set formulation for this flow. The evolution is defined as

$$\mathcal{S}_t = |\kappa|^{\frac{1}{4}} \vec{N} \quad (13)$$

where  $\kappa$  is the Gaussian curvature and  $\vec{N}$  is the Euclidean normal. We take the positive part of the Gaussian curvature because it might be negative. This extension to non-convex surfaces was established and justified in [10, [2]] by Alvarez *et. al.*.

We have defined all the necessary flows for our implementation and experiments. Table 1 summarizes the evolution equations. We now look at the important mathematical properties of these flows.

## 3 Mathematical Properties

Even though the flows are governed by local curvature estimates, the evolution develops a number of interesting global properties. In the literature, the key properties were first discovered by considering the problem on convex curves. Then, proofs were extended to non-convex curves because it was proved that a non-convex curve evolves smoothly to a convex one without developing any singularities. Thus, all the important properties also hold for non-convex curves. In the Euclidean space, this work was the contribution of Gage and Hamilton [3] and then Grayson did the proofs for non-convex curves in [4]. In affine geometry, a similar situation occurred. First, Alvarez *et. al* and Sapiro and Tannenbaum independently showed the characteristics of the affine flow on convex curves. Then, Angenent, Sapiro and Tannenbaum treated the non-convex case in [9].

Properties	Short Explanation
1. Order-preserving smoothing	Two disjoint curve remain disjoint in the smoothing process. The curves will never cross even if one is inside the other.
2. Smooth smoothing	Curves last for a finite time. They evolve to a convex curve, remain convex in time and then converge to a round point following the Euclidean flow or to an elliptical point under the affine flow. All this without developing self-intersection or creating singularities.
3. Decreasing total curvature	The undulation of a curve is decreasing in the smoothing process.
4. Decreasing number of inflection and extrema points	No new extremas or inflection points can be created in the smoothing process.
5. Iterative smoothing	The semi-group property holds, i.e. $T(t_1 + t_2) = T(t_1)T(t_2)$ , for scale parameters $t_1$ and $t_2$ .

Table 2: Key properties of the Euclidean and affine geometric heat flows

Table 2 summarizes the key properties of the smoothing evolutions by curvature deformation. The proofs are instructive but we do not get into their details as it is not the purpose of this work. They are mostly based on some version of the maximum principle of parabolic equation and the  $\delta$ -Whisker lemma which basically states that a curve cannot get closer than a distance  $\delta$  to itself [3], [4]. Also, an important contribution of Hamilton was to show the non-existence of corners during evolution because the curvature estimate cannot become unbounded (blow up) on arcs which turn through an angle less than  $\pi$ .

We deal with the Euclidean and affine case at the same time as all properties apply to both flows. The only difference is in property 2 where, in the limit, Euclidean flow converges to a circular point whereas the affine evolution moves to an elliptical point. Furthermore, note that property 4 and 5 are the *causality* and the *semi-group* properties. Hence, both the Euclidean and the affine flows presented describe a scale-space.

The stated properties are all very important to justify the utilization of the flows for smoothing images because smoothing of an image is based on viewing the image as a collection of iso-intensity level curves where each is evolved according to the curvature deformation equations. Thus, all the nice properties of Table 2 act independently on each intensity level curve of the image. This will be illustrated with movies and figures in the experiment section.

In 3D, all properties stated above collapse for non-convex surfaces. It is not true that the flows evolve without creating new structure. There are many examples where we see the surface splitting apart and creating discontinuities when it was initially connected. The situation of non-convex surfaces is very complicated and still the subject of much research. However, properties do hold for convex surfaces as we will note later in the experiment section.

## 4 Level Set Formulation of the Flows

The smoothing of shape by curvature deformation can be extended to smoothing images. In 2D, the curve evolutions are implemented as the evolution of a surface which embeds the curve as its zero level set. In 3D, a four dimensional hyper-surface is evolved with the surface embedded as its zero level set. Recall that any continuous function can be used for this higher dimensional embedding function. Also, we can choose any level set in the evolution [5]. Hence, in image denoising, we simply smooth by mean curvature or affine curvature each iso-intensity level set of the image and then superimpose them to get a resulting smoothed image [1]. But why is it sound to do this? Evans and Spruck's paper [2] investigates this question for the mean curvature level set formulation

$$\psi_t = |\nabla\psi| \operatorname{div} \left( \frac{\nabla\psi}{|\nabla\psi|} \right) \quad (14)$$

where at  $t = 0$ ,  $\psi = \psi_0$ , is the initial surface. In our case, this corresponds to the image intensity function. They prove a few results to conclude that the flow is well-posed, stable and applicable on images as even if the gradient of  $\psi$  is undefined or zero at some points, a weak solution exists which matches with the classical solution at points where there is no problem with the gradient of  $\psi$ . This allows us to consider images and shapes with corners and discontinuities. Numerically, this weak solution is achieved by introducing a small  $\epsilon$  parameter in the denominator. In 2D, we get

$$\psi_t = \frac{\psi_{xx}\psi_y^2 - 2\psi_x\psi_y\psi_{xy} + \psi_{yy}\psi_x^2}{\psi_x^2 + \psi_y^2 + \epsilon} \quad (15)$$

We obtain a similar expression for surface evolution. It is specified in [5].

The affine version turns out to have an elegant level set form due to the exponent of the curvature term. In 2D, because of the 1/3 exponent, the gradient denominator vanishes completely. We have

$$\psi_t = (\psi_{xx}\psi_y^2 - 2\psi_x\psi_y\psi_{xy} + \psi_{yy}\psi_x^2)^{\frac{1}{3}} \quad (16)$$

In [11], based on the theory of viscosity solutions, Olver, Sapiro and Tannenbaum argue that even if the level sets are non-smooth, the flow is well-posed and stable. The maximum principle holds meaning that the flow is smoothing images. Furthermore, it is shown that the 1/3 power is the unique one to eliminate the denominator term. This makes the numerical implementation more stable.

A similar situation happens with the 3D affine curvature deformation. Recall that we use the Gaussian curvature of the surface. It has a squared gradient denominator which implies that when raised to the power 1/4 and multiplied with the normal expression, the denominator term vanishes again. We obtain,

$$\psi_t = \left| \begin{array}{l} (\psi_{yy}\psi_{zz} - \psi_{yz})\psi_x^2 + (\psi_{xx}\psi_{zz} - \psi_{xz})\psi_y^2 + (\psi_{xx}\psi_{yy} - \psi_{xy})\psi_z^2 + \\ + 2\psi_x\psi_y(\psi_{xz}\psi_{yz} - \psi_{xy}\psi_{zz}) + 2\psi_y\psi_z(\psi_{xy}\psi_{xz} - \psi_{yz}\psi_{xx}) \\ + 2\psi_x\psi_z(\psi_{xy}\psi_{yz} - \psi_{xz}\psi_{yy}) \end{array} \right|^{\frac{1}{4}} \quad (17)$$

The 1/4 exponent is also the unique one that will eliminate the denominator of the affine surface evolution.

## 5 Implementation

The implementation is straight forward for smoothing applications. We do not need to compute any complicated initial higher dimensional embedding function as we are simply using the intensity function of images. We then move every point according to the obvious discretized version of equations (14)-(17). Since the flows are well-behaved and do not develop any singularities, we can use a simple central difference method to compute the first and second order derivatives. We use a three neighbor support approximation as suggested in appendix A.2 of [14]. Finally, we must set several parameter values. We typically choose a very small  $\epsilon$  in the order of  $10^{-10}$ . For the Euclidean flow, a time step of 0.1 was used in 2D whereas in the affine curve evolution, we used a time increment of 0.01. We found the surface evolutions much more unstable in practice. We had to use a time step of  $10^{-3}$  in the Euclidean mean curvature case and  $10^{-6}$  in the affine equations in order to get relatively stable surface flows. Lastly, the duration of the evolution is needed as input. Therefore, the 3D experiments take very long to terminate as the increment in time is very small.

## 6 Experimental Results

The experiment is organized in three parts. First, we illustrate the nice mathematical properties of both the Euclidean and the affine evolutions on 2D curve evolutions. Then, we see how these important characteristics can be applied to smooth each iso-intensity level set of images. We show the flows on a retinal angiogram and have tested the evolutions on 3D MRI brain images. Finally, we demonstrate how the properties extend well to convex surfaces but fail on non-convex surfaces with the classical barbell example. All the figures and movies related to the Euclidean mean curvature deformation are presented at [www.cim.mcgill.ca/~mdesco/mean.html](http://www.cim.mcgill.ca/~mdesco/mean.html). Similarly, results obtained using the affine curvature deformation are at [www.cim.mcgill.ca/~mdesco/affine.html](http://www.cim.mcgill.ca/~mdesco/affine.html). It is worth opening these pages while reading this section of the report.

## 6.1 Curve Evolutions

We present several evolutions illustrating the main properties of Table 2. For this experiment, we slightly extended the software created by Alexander Vasilevskiy for his Masters thesis. We just incorporated the affine curvature evolution. We first show a convex curve example of the ellipse. Note that the ellipse stays more elliptical under the affine flow before converging to a point and vanishing. Then, we have three non-convex curve examples. Note how the curves first evolve to a convex curve without creating singularities. This is because the inflection points stay fixed, concavities move outward and convexities move inward. This is clearer on the second movie. The star example illustrates that we can consider shapes with corners. Note how the initial star has sharp corners that are rapidly smoothed. Finally, the spiral example illustrates the maximum principle and the  $\delta$ -Whisker lemma presented in [4] Grayson. It is impressive to see how the spiral never comes closer to itself than it was originally.

## 6.2 Smoothing Images

In this part of the experiment, we smooth 2D and 3D images. On the result html pages, we only show 2D images. To present 3D results, we would need to choose certain slices of the 3D data. We visualize the 3D smoothed data with medical imaging tools of the Montreal Neurological Institute (MNI), *register* or *Display*.

We first present the image of a cat lying on a carpet. Ideally, we would like to smooth out the carpet small structures and keep the important features of the cat. This is exactly what happens in both the Euclidean and the affine case. It is interesting to see the evolution of the 75 and 150 iso-intensity level curves. We see that the small curves representing the carpet are quickly smoothed away. A good duration seem to be 8 units as the cat now appears to be lying on a uniform gray background while its important information like eyes, mouth, tail, and paws are preserved.

Then, we show a retinal angiogram where there are many blood vessels of different size. Note that the original image contains artifacts and small white speckle dots. In practice, this is what we want to remove before attempting any segmentation or blood vessel recovery algorithm. We observe that the evolutions do perform the desired task while keeping the blood vessels, even the small thin ones. The resulting smoothed images are quite similar in both the Euclidean and affine case. We have further tested the flows on 3D MRI images of the brain. Both evolutions have been implemented so that we can execute them at the MNI with the proper medical image formats and libraries. Again, we observe that both flows behave quite similarly although, by eye, the affine curvature deformation seem to be maintaining the blood vessels intact for a longer period of time.

## 6.3 Surface Evolutions

Finally, we have tested the flows on simple volumes to illustrate the extensibility of the mathematical properties of Table 2 to 3D space. In the Euclidean mean curvature flow, we note that the characteristics are respected on convex surfaces like the sphere and the tube.

These two examples both evolve smoothly. However, we see with the barbell and perturbed filament movies that breaking and splitting apart can occur on non-convex volumes. Discontinuities and new structure are introduced. This agrees with the theory presented in the literature related to surface evolution under the mean curvature flow [2].

On the other hand, the affine curvature flow behaves quite differently. First, note that points on the tube do not evolve at all except for some unstable points at the extremities. Why? Recall that the flow is based of the Gaussian curvature estimate. From basic differential geometry, we know that for all points on a cylindrical volume one of the principal curvature is zero. Thus, the Gaussian curvature vanishes and there is no evolution. This is most probably an explanation for our qualitative observation that MRI images containing cylindrical structure like blood vessels are left intact longer under the affine flow than under the Euclidean geometric heat flow.

We also present the classic barbell evolution. In theory, Caselles and Sbert have shown in [10, [14]] that the barbell does not become singular under the presented affine surface flow. However, we observe in our implementation that the surface splits apart. Like the tube, the bar handle should not move at all. However, it does shrink at the end points of the bar. This causes the surface to break apart and move inward before vanishing completely. We believe this is in part due to our manually generated barbell volume which is not perfect. Also, it is clear that discretization and numerical approximations can cause significant problems.

## 7 Discussion and Conclusion

We have presented the theory and the implementation of the Euclidean geometric heat equation and the affine curvature deformation analogue. This was done by introducing the sufficient affine differential geometry concepts and discussing the important issues of the evolution equations. In particular, we questioned a statement made by Sapiro and Tannenbaum and have attempted to correct it. We argued that it is invalid to say that the affine flow,  $\mathcal{C}_t = C_{ss}$ , shrinks the affine length as quickly as possible. Then, we saw the implementation details of the flows. They are easily implemented using level set methods. We clearly see that both have important properties that make them very useful for medical image processing. They are both excellent methods to remove unwanted artifacts and noise while preserving the important structures of the image.

But which one of the two should we use in practice? Based on our experiment, we observed that the affine flow was a better candidate for a few reasons. Not only is it analytically nicer, it is numerically easier to implement mainly because there cannot be any problem with the denominator blowing up. Hence, it was found to be more stable than the Euclidean mean curvature evolution. Furthermore, we see that the affine flow seem to be maintaining the blood vessel for a longer time than the Euclidean flow evolution. This phenomenon has also been observed on brain images by Olver, Sapiro and Tannenbaum. They claim the elliptical structures of the brain (blood vessels) were preserved up to a higher degree of smoothing using the affine flow. They don't show how they got to this conclusion but in our case, this observation is made qualitatively only by analyzing the smoothed images by eye.

Moreover, Olver, Sapiro and Tannenbaum state that a comparison between the Euclidean

and the affine flows was done in a technical report [10, [46]] showing that the affine flow was better at denoising MRI images. We wonder how this comparison was done. It is not obvious and clear to us how to go about rigorously showing that one evolution equation is performing better than the other. First of all, the flows are numerically implemented with different parameters. This is because they behave differently and for instance, need a specific choice of time step to make sure the evolutions are stable. Also, what does it mean for a flow to perform better? A proper definition is needed and a regularized way to compute the amount of preserved structure must be established.

This comparison problem is interesting and is worth exploring in future work. We need to read the existing literature related to this matter. It would be nice to propose a framework to process brain images which would select the best smoothing procedure depending on the application.

**Acknowledgments** This work was supported by Kaleem Siddiqi and the Center for Intelligent Machines at McGill University. Special thanks to Kaleem Siddiqi and Pavel Dimitrov for several interesting discussions and to Allen Tannenbaum for quick electronic replies. Finally, the presented experimental results would not have been possible without the software support of Alexander Vasilevskiy.

## References

- [1] B. B. Kimia & K. Siddiqi “Geometric Heat Equation and Nonlinear Diffusion of Shapes and Images.” *Computer Vision and Image Understanding*, vol. 64, no. 3, November, pp. 305-322, 1996.
- [2] R. C. Evans & J. Spruck “Motion of Level Sets by Mean Curvature I,” *I. J. Diff. Geom.*, vol. 33, pp. 635-681, May 1991.
- [3] M. Gage & R. S. Hamilton “The heat equation shrinking convex plane curves,” *J. Diff. Geom.*, vol. 23, pp. 69-96, 1986.
- [4] M. A. Grayson “The heat equation shrinks embedded plane curves to round points,” *J. Diff. Geom.*, vol. 29, pp. 285-314, 1987.
- [5] J.A. Sethian “Level Set Methods,” *Cambridge University Press*, Chapter 1,2, and 5, 1996.
- [6] G. Sapiro & A. Tannenbaum “Affine Invariant Scale-Space” *International Journal of Computer Vision*, vol. 10, pp. 25-44,1993.
- [7] G. Sapiro & A. Tannenbaum “On Affine Plane Curve Evolution” *Journal of Functional Analysis*, vol. 119, pp. 79-120,1994.
- [8] G. Sapiro & A. Tannenbaum “Area and Length Preserving Geometric Invariant Scale-Spaces” *IEEE trans. Pattern Analysis and Machine Intelligence*, vol. 17, no. 1, pp. 67-72, 1995.

- [9] S. Angenent, G. Sapiro & A. Tannenbaum “On the affine heat equation for non-convex curves” *J. of the American Mathematical Society* vol. 11, no. 3, pp. 601-634, 1998.
- [10] Peter J. Olver, G. Sapiro & A. Tannenbaum “Invariant Geometric Evolutions of Surfaces and Volumetric Smoothing” *J. Appl. Math* vol. 57, no. 1, pp. 176-194, 1997.
- [11] Peter J. Olver, G. Sapiro & A. Tannenbaum “Affine invariant detection: edge maps, anisotropic diffusion, and active contours” *Acta Appl. Math.* vol. 59, pp. 45-77, 1999.
- [12] E. Calabi, Peter J. Olver & A. Tannenbaum “Affine Geometry, Curve Flows, and Invariant Numerical Approximations” *Advances in Mathematics* vol. 124, pp. 154-196, 1996.
- [13] H. W. Guggenheimer “Differential Geometry” *McGraw-Hill Book Company*, New York, 1963.
- [14] E. Trucco & A. Verri “Introductory Techniques for 3-D Computer Vision” *Prentice-Hall*, 1998.
- [15] K. Siddiqi, Y. B. Lauziere, A. Tannenbaum & S. W. Zucker “Area and Length Minimizing Flows for Shape Segmentation” *IEEE transactions on Image Processing*, vol. 7, no. 3, March 1998.